PNAS PLUS

Suppression of NF-κB activity via nanoparticle-based siRNA delivery alters early cartilage responses to injury

Huimin Yan[a,1], Xin Duan[b,c,1], Hua Pan[d], Nilsson Holguin[c], Muhammad Farooq Rai[c], Antonina Akk[a], Luke E. Springer[a], Samuel A. Wickline[d,2], Linda J. Sandell[c,2], and Christine T. N. Pham[a,2]

[a]Division of Rheumatology, Department of Medicine, Washington University School of Medicine, St. Louis, MO 63110; [b]Orthopedics Department, The First Affiliated Hospital of Sun Yet-Sen University, Guangzhou, China, 510080; [c]Department of Orthopedic Surgery, Washington University School of Medicine, St. Louis, MO 63110; and [d]Division of Cardiology, Department of Medicine, Washington University School of Medicine, St. Louis, MO 63110

Edited by Virginia B. Kraus, Duke University, Durham, NC, and accepted by Editorial Board Member Mark E. Davis August 22, 2016 (received for review May 23, 2016)

Osteoarthritis (OA) is a major cause of disability and morbidity in the aging population. Joint injury leads to cartilage damage, a known determinant for subsequent development of posttraumatic OA, which accounts for 12% of all OA. Understanding the early molecular and cellular responses postinjury may provide targets for therapeutic interventions that limit articular degeneration. Using a murine model of controlled knee joint impact injury that allows the examination of cartilage responses to injury at specific time points, we show that intraarticular delivery of a peptidic nanoparticle complexed to NF-κB siRNA significantly reduces early chondrocyte apoptosis and reactive synovitis. Our data suggest that NF-κB siRNA nanotherapy maintains cartilage homeostasis by enhancing AMPK signaling while suppressing mTORC1 and Wnt/β-catenin activity. These findings delineate an extensive crosstalk between NF-κB and signaling pathways that govern cartilage responses postinjury and suggest that delivery of NF-κB siRNA nanotherapy to attenuate early inflammation may limit the chronic consequences of joint injury. Therapeutic benefits of siRNA nanotherapy may also apply to primary OA in which NF-κB activation mediates chondrocyte catabolic responses. Additionally, a critical barrier to the successful development of OA treatment includes ineffective delivery of therapeutic agents to the resident chondrocytes in the avascular cartilage. Here, we show that the peptide–siRNA nanocomplexes are nonimmunogenic, are freely and deeply penetrant to human OA cartilage, and persist in chondrocyte lacunae for at least 2 wk. The peptide–siRNA platform thus provides a clinically relevant and promising approach to overcoming the obstacles of drug delivery to the highly inaccessible chondrocytes.

posttraumatic osteoarthritis | nanomedicine | siRNA | NF-κB | autophagy

Osteoarthritis (OA) is the most common form of arthritis and a major cause of morbidity in the aging population (1). Currently, there are limited treatment options and no disease-modifying OA drugs (DMOADs). Joint injury is a known predisposing factor for the development of posttraumatic OA (PTOA) and accounts for 12% of all OA in the United States, costing more than $3 billion annually in healthcare (2). Surgical stabilization alone does not prevent PTOA development (3). Several studies have documented a robust inflammatory response in the aftermath of joint injury that likely contributes to chondrocyte death and cartilage degeneration (4). These observations suggest that limiting the early inflammatory responses may retard PTOA development. Understanding the molecular and cellular responses postinjury may also provide targets for therapeutic interventions that limit articular degeneration, a characteristic of all forms of OA.

However, detection of the early events in chondrocyte responses that lead to cartilage degeneration has been difficult to accomplish. To gain further insights into these early events, we established a noninvasive model to induce cartilage injury by applying controlled compressive loads to mouse knee joint (5). This model allows the examination of molecular and structural events at specific time points postinjury. We hypothesize that early interruption of the inflammatory cascade postinjury will halt the progression of cartilage damage. We also posit that the NF-κB pathway represents an attractive therapeutic target for PTOA prevention, as its activity controls the expression of gene products involved in a myriad of cellular responses and is essential for the expression of catabolic mediators in OA cartilage and synovium (6).

Although local [intraarticular (i.a.)] delivery of therapeutic agents represents an attractive approach for the treatment of OA, as it is potentially safer and more effective than systemic administration, drug delivery into subcompartments of cartilage has proven a challenging task (7). The avascular cartilage renders chondrocytes inaccessible even to locally delivered therapeutics, and the dense collagen matrix further prevents effective drug penetration into the deeper cartilage layers. In these proof-of-concept studies, we used a peptidic nanoparticle (NP) structure that features an amphipathic, cationic, cell-penetrating peptide as an siRNA carrier that is stable in biological fluids and enables coordinated endosomal escape and release of siRNA into the cytoplasm to rapidly engage the RNA-induced silencing complex and simultaneously suppresses both canonical and noncanonical NF-κB activities (8, 9). We have recently shown that these peptide–siRNA nanocomplexes suppressed inflammation in a preclinical model of rheumatoid arthritis by downregulating NF-κB p65 expression specifically in the joints without affecting p65 expression or host immune responses in off-target organs (10). Here, we show that administration of peptide–NF-κB

Significance

Osteoarthritis is a common debilitating joint disease that affects millions in the United States and for which there are few therapeutic options. Critical barriers to the successful development of osteoarthritis treatment include limited understanding of the pathways governing early cartilage degradation and ineffective delivery of therapeutic agents to the resident chondrocytes in the avascular cartilage. Using a peptidic nanoparticle carrying siRNA that specifically suppresses NF-κB, we show that early antiinflammatory intervention reduces chondrocyte death caused by joint injury, a known predisposing factor for osteoarthritis. The peptidic nanoparticle deeply penetrates human cartilage to deliver its therapeutic cargo to the chondrocytes, demonstrating its ability to permeate the dense cartilage matrix. This approach promises to overcome the barriers to effectively treat osteoarthritis.

Author contributions: H.P., S.A.W., L.J.S., and C.T.N.P. designed research; H.Y., X.D., H.P., N.H., A.A., and L.E.S. performed research; H.P., M.F.R., S.A.W., and L.J.S. contributed new reagents/analytic tools; and H.Y., X.D., H.P., M.F.R., S.A.W., L.J.S., and C.T.N.P. wrote the paper.

Conflict of interest statement: Samuel Wickline has equity in Trasir Therapeutics, Inc.

This article is a PNAS Direct Submission. V.B.K. is a Guest Editor invited by the Editorial Board.

[1]H.Y. and X.D. contributed equally to this work.

[2]To whom correspondence may be addressed. Email: wicklines@aol.com, sandelll@wudosis.wustl.edu, or cpham@wustl.edu.

This article contains supporting information online at www.pnas.org/lookup/suppl/doi:10.1073/pnas.1608245113/-/DCSupplemental.

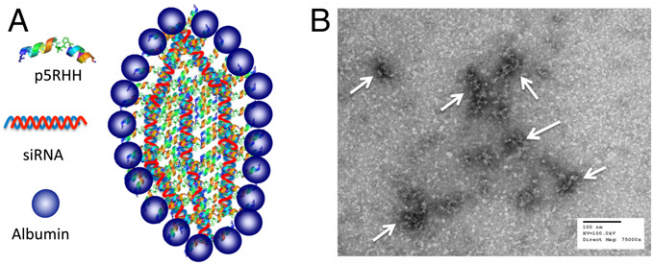

Fig. 1. p5RHH-siRNA nanoparticles. (*A*) A schematic illustration of p5RHH-siRNA nanoparticles with albumin coating. (*B*) Transmission electron micrograph of p5RHH-siRNA nanoparticles.

siRNA NP immediately postinjury significantly reduces chondrocyte apoptosis and reactive synovitis while maintaining cartilage homeostasis. We also establish that the NP freely and deeply penetrates human cartilage, persisting in chondrocyte lacunae for at least 2 wk.

Results

Formulation and Characterization of Peptide–siRNA NP. We have previously reported that the cationic amphipathic peptide designated as "p5RHH" (VLTTGLPALISWIRRRHRRHC) is capable of siRNA transfection without significant cytotoxicity at all tested doses (8). This novel sequence lacks the toxicity profile of its full parent compound, melittin, because it features a truncation of six terminal amino acids that prevents peptide-induced cytolytic membrane pore formation at low doses in the blood stream (11–13), yet when concentrated in endosomes still promotes endosomolysis and siRNA escape (9). The noncovalent coupling, self-assembling formulation strategy is depicted in Fig. 1*A*, where p5RHH (10 mM) is mixed with siRNA (100 μM) at 100:1 peptide:siRNA ratio in dilution buffer (HBSS) followed by incubation at 37 °C for 40 min or on ice for 10 min. At this point, the size of p5RHH-siRNA NP is ∼55 nM by wet mode atomic force microscopy (8, 9) and by transmission electron microscopy (TEM) (Fig. 1*B*). The NP was fully stabilized for later injection by mixing with albumin, where albumin final concentration was 0.5 mg/mL, or was used immediately without a stablization step.

Effects of p5RHH–NF-κB siRNA NP on Cartilage Following Impact Injury. We used a noninvasive murine model of controlled knee-joint impact injury delivered by axial tibial compression consisting of a single loading episode of 60 cycles (5). This injury model allows for the study of early events after impact, at a time when inflammation is thought to be particularly important, and mimics a traumatic joint injury (5). Although we observed no NF-κB activity in the absence of injury, mechanical loading stimulated both canonical (p65) and noncanonical (p100) pathways (Fig. 2*A*). Phosphorylation of p65 was detected as early as 12 h following joint injury at and around the impact site and persisted for at least 2 wk. On the other hand, significant p100 activation was not observed until at least 48 h after loading (Fig. 2*A*). Impact injury also led to NF-κB up-regulation in the synovium (Fig. 2*A*). Although previous studies suggested that the canonical pathway of NF-κB signaling plays a central role in the catabolic responses of OA cartilage (6), the exact contribution of the noncanonical pathway to chondrocyte pathology has not been evaluated. We initially hypothesized that a

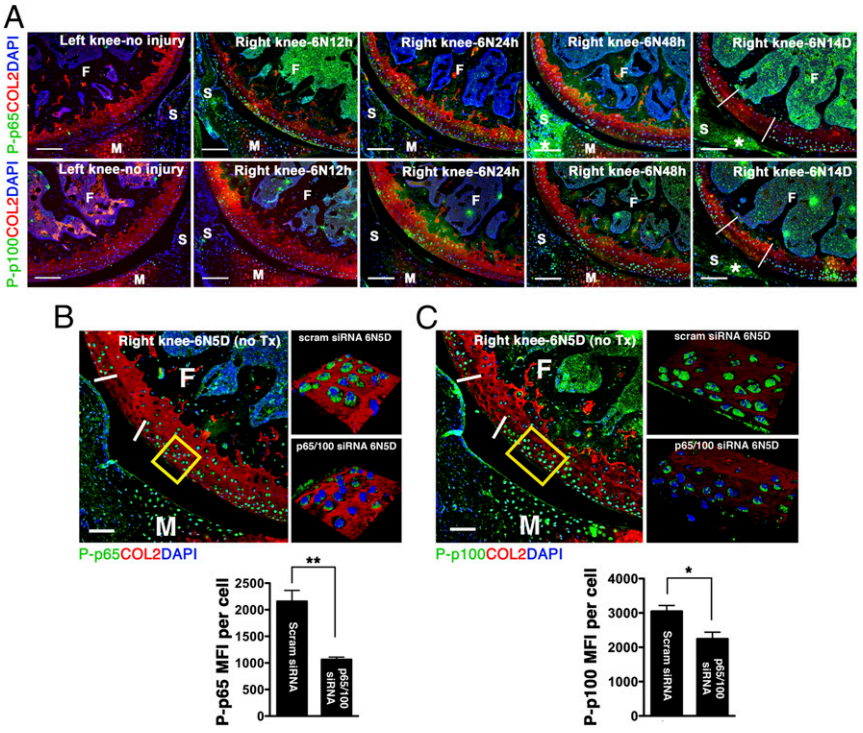

Fig. 2. NF-κB expression following joint injury and p5RHH–NF-κB siRNA NP treatment. (*A*) Mouse knee joints were loaded with 6 N on day 0 and examined for phospho (P)-p65 (green, *Upper*) and P-p100 (green, *Lower*) at the indicated time. There is no p65 or p100 phosphorylation in the left, uninjured knee. Phosphorylation of p65 is seen at and around the impact area as early as 12 h after impact injury and persists for at least 14 d outside of the impact area (white demarcation lines) and in the synovium (*). p100 phosphorylation is delayed, becoming notable around 48 h and persisting until day 14. Mice were left untreated or injected i.a. with p65 and p100 siRNA NP immediately and at 48 h after impact injury; knees were harvested on day 5 for analysis. Mean fluorescent intensity (MFI) of P-p65 (*B*) and P-p100 (*C*) per chondrocyte in p5RHH–NF-κB siRNA NP or scrambled (scram) siRNA NP-treated knees was measured in the boxed area just outside of the impact zone (demarcated by white lines) from z-stack confocal images. Values represent mean ± SEM. $n = 4$ mice per treatment group. $^{*}P < 0.05$; $^{**}P < 0.01$. (Scale bars, 100 μm.) COL2 (red), type II collagen; F, femur; M, meniscus; S, synovium; T, tibia; Tx, treated. DAPI (blue) stains nuclei.

combinatorial RNA-silencing strategy aimed at dual inhibition of p65 and p100 would be superior to targeting individual pathways.

Informed by the articular dwelling time of the p5RHH-siRNA NP (Fig. S1) and the timing of p65/p100 up-regulation following impact injury (Fig. 2*A*), we elected to administer a combination of p5RHH-p65/p100 siRNA NPs i.a. (0.05 μg of each siRNA for a total of 0.1 μg in a volume of 15 μL, which was equivalent to 7.5×10^{-12} mol of siRNA) immediately after compression injury and repeated the i.a. injection at 48 h in an attempt to simulate early preventative therapy in a real clinical setting. p5RHH-scrambled siRNA NP (0.1 μg) served as control. On day 5, knee joints were dissected and processed for histology and immunostaining. We observed significant decrease in phosphorylation of p65 and p100 in chondrocytes, ∼50% and ∼30%, respectively, which was still evident 72 h after the last NF-κB siRNA NP administration (day 5, Fig. 2 *B* and *C*). In addition, p5RHH-p65/p100 siRNA NPs limited chondrocyte death, as evidenced by an ∼50% reduction in the number of TUNEL$^+$ chondrocytes (Fig. 3*A*). Suppression of p65/p100 phosphorylation and chondrocyte death correlated with an ∼40% reduction in cartilage injury length (lesion) as measured by the extent of proteoglycan loss, which was indicated by reduction in Safranin O staining (Fig. 3 *B* and *C*). Mechanical loading also changed the distribution pattern of aggrecan from pericellular to intracellular in the area of impact injury, as previously described (5) (Fig. S2). Areas with aggrecan redistribution corresponded to areas of dying cells (TUNEL$^+$ cells) (Fig. S2) and correlated with cartilage injury length measured by loss of Safranin O staining (Fig. 3 *B* and *C*). In addition, p5RHH–NF-κB siRNA NP i.a. administration also profoundly suppressed p65/p100 phosphorylation in the synovium (Fig. S3), which likely explains the ∼40% reduction in posttraumatic reactive synovitis as measured by a previously established scoring system (5) (Fig. 3 *B* and *C*).

To evaluate the specific effects of p65 versus p100 suppression, we treated separate sets of mice with either i.a. p5RHH-p65 siRNA NP (0.05 μg) or p5RHH-p100 siRNA NP (0.05 μg), using the same delivery schedule as above. We showed that the gene-silencing effect was specific to respective siRNA (Fig. 4 *A* and *B*). Suppression of either p65 or p100 reduced the number of TUNEL$^+$ cells, cartilage injury length (extent of proteoglycan loss), and reactive synovitis (Fig. 4*C*) although only the p65 suppression was significantly reduced compared with no treatment. Results showed that combined inhibition of p65 and p100, although statistically different from no treatment, did not provide additional protection compared with the suppression of p65 alone (Fig. 4*C*). These findings suggest that the canonical p65 pathway plays a major role in cartilage response following impact injury.

Effects of p5RHH–NF-κB siRNA NP on Chondrocyte/Cartilage Homeostasis. Normal chondrocytes express high levels of autophagy-related genes (Atg), such as microtubule-associated protein light chain 3 (LC3), whereas aging and osteoarthritic cartilage displays marked reduction in Atg expression accompanied by increased apoptosis (14, 15). We observed that impact injury significantly reduced chondrocyte-associated LC3 expression, an event that occurred as early as 12 h after injury and became more extensive over time (Fig. 5*A*). Treatment with p5RHH-p65/p100 siRNA NPs limited the injury-induced suppression of LC3 expression, an ∼40% reduction at day 5 (Fig. 5*B*), suggesting that NF-κB signaling also modulates

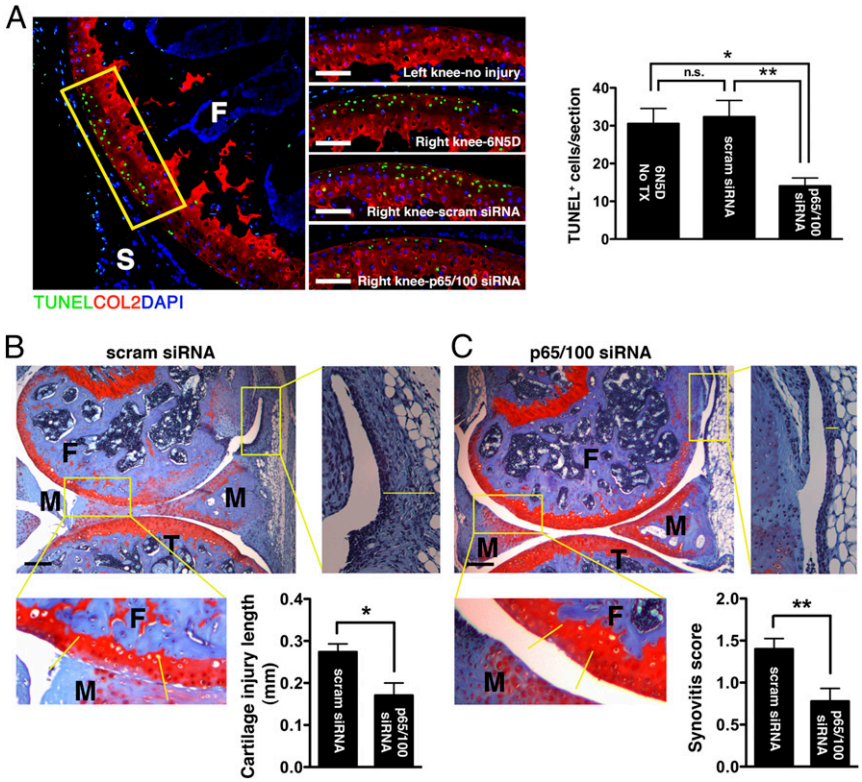

Fig. 3. Effects of dual p5RHH-p65/p100 siRNA NP treatment on the severity of cartilage damage and reactive synovitis. Mouse knees were subjected to compression injury at 6 N and injected i.a. with 0.1 μg of p65/p100 siRNA combined or scrambled (scram) siRNA NP immediately and at 48 h postinjury. (*A*) On day 5, knees were processed and examined for TUNEL staining (green) in the impact area (rectangle). The number of TUNEL$^+$ cells was enumerated across the entire impact area (spanning 50- × 5-μm slides) and expressed as mean cell number per section. Comparison of the length of cartilage lesion (based on loss of Safranin O staining between yellow demarcation lines) and reactive synovitis (yellow line) in p5RHH-scram siRNA NP-treated (*B*) and in p5RHH-p65/p100 siRNA NP-treated (*C*) knees. Values represent mean ± SEM. $n = 4$ mice per treatment group. COL2 (red), type II collagen; F, femur; M, meniscus; T, tibia; Tx, treatment. DAPI (blue) stains nuclei. [Scale bars, 100 μm (*A*) and 250 μm (*B* and *C*).] *$P < 0.05$; **$P < 0.01$; n.s., not significant.

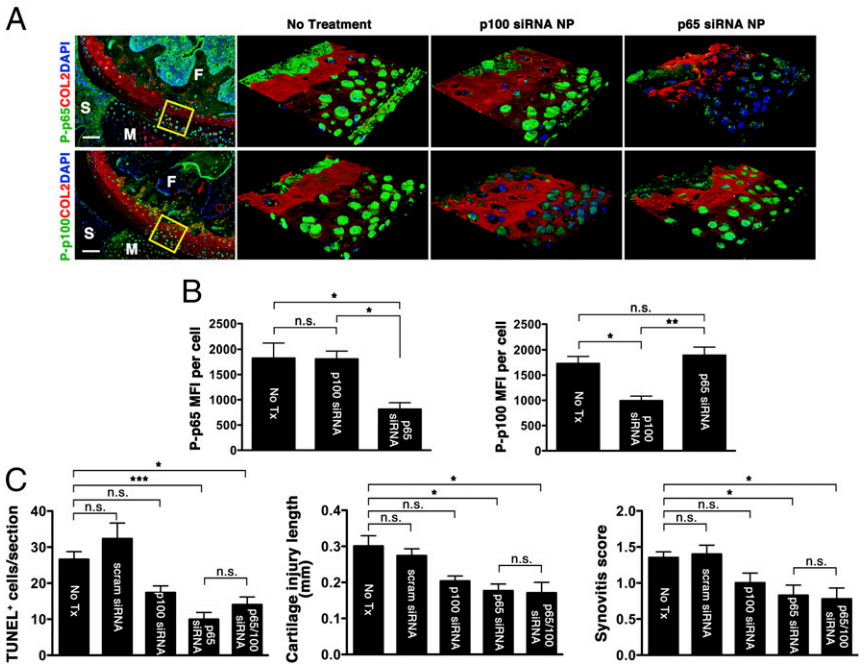

Fig. 4. Effect of individual p5RHH-p65 and p5RHH-p100 siRNA NP treatment. Mouse knees were subjected to compression injury at 6 N and left untreated (No Tx) or injected i.a. with 0.05 μg of p5RHH-p65 or p100 siRNA NP immediately and at 48 h postinjury. (*A*) On day 5, knees were processed and examined for P-p65 and P-p100 in the boxed area by confocal microscopy. (*B*) MFI of P-p65 (*Left*) and P-p100 (*Right*) expression level per chondrocyte was analyzed from z-stack confocal images. (*C*) The number of TUNEL$^+$ cells, length of cartilage lesions (based on loss of Safranin O staining), and reactive synovitis in the different treatment groups. Values represent mean ± SEM; $n = 4$ mice per treatment group. *$P < 0.05$; **$P < 0.01$; ***$P < 0.001$; n.s., not significant. (Scale bars, 100 μm.)

chondrocyte autophagy. The relationship between NF-κB and autophagy in cell death/survival in the context of cancers is well described (reviewed in refs. 16 and 17). How NF-κB signaling may modulate autophagy to maintain chondrocyte homeostasis is still unknown. We hypothesized that NF-κB suppression promotes chondrocyte autophagic activity through the inhibition of mammalian target of rapamycin (mTOR), a known negative regulator of autophagy (18). To this end we treated another set of mice with an i.a. injection of p5RHH-p65 siRNA NP or scrambled siRNA NP immediately after impact loading and examined the knee joints at 24 h. Consistent with the data obtained at day 5 (Fig. 3*A*), p5RHH-p65 siRNA NP reduced the number of TUNEL$^+$ cells within 24 h by ∼50% whereas p5RHH-scrambled siRNA NP had no effect (Fig. S4*A*). We further confirmed that chondrocyte death proceeded in part through apoptosis, as evidenced by nuclear localization of poly(ADP ribose) polymerase (PARP) C-terminal cleavage fragment (Fig. S4*B*). In addition, we found that impact injury up-regulated mTOR phosphorylation in chondrocytes whereas p5RHH-siRNA NP administration significantly suppressed mTOR complex 1 (mTORC1) activity, as evidenced by attenuation of ribosomal protein S6 phosphorylation downstream of mTOR (Fig. 6*A*). Taken together, these results suggest that p5RHH- p65

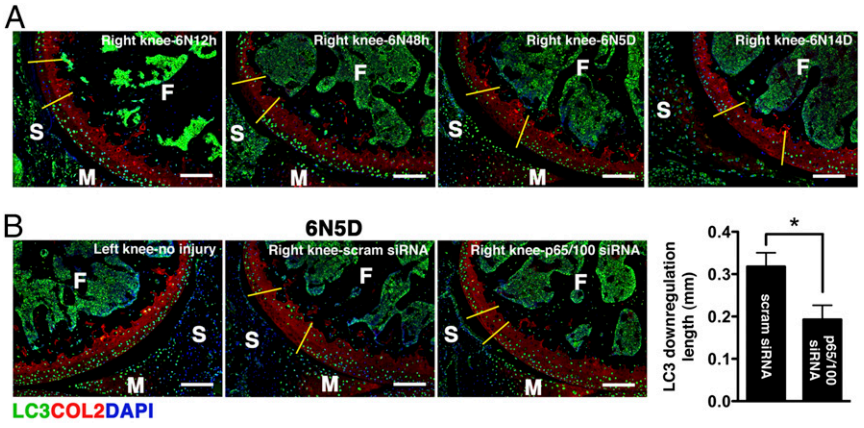

Fig. 5. Effect of dual p5RHH-p65/p100 siRNA NP treatment on autophagy. (*A*) Mice were subjected to compression injury at 6 N, and LC3 expression was assessed over time. (*B*) Injured knees were injected i.a. with 0.1 μg of p5RHH-p65/100 siRNA NPs or p5RHH-scrambled (scram) siRNA NPs immediately and at 48 h postinjury; the knees were harvested at day 5 postinjury and examined for LC3 expression (green). The length of LC3 down-regulation was evaluated across the entire impact area; the section with the longest length (of LC3 suppression) was selected and measured using ImageJ. Values represent mean ± SEM; $n = 4$ mice per treatment (Tx) group. COL2 (red), type II collagen; F, femur; M, meniscus; S, synovium. DAPI (blue) stains nuclei. (Scale bars, 100 μm.) *$P < 0.05$.

siRNA NP preserved chondrocyte autophagy/homeostasis via suppression of mTORC1 activity.

It is known that mTORC1 activity is regulated by AMP-activated protein kinase (AMPK) (18–20), a potent inducer of autophagy. Recent evidence also suggests that AMPK is constitutively phosphorylated at Thr^{172} in articular cartilage and that the phosphorylation decreases with OA (21, 22). Thus, we explored the possibility that p5RHH-p65 siRNA nanotherapy suppressed mTORC1 via AMPK activation. Indeed, we found that AMPK activity was maintained in the noninjured knee whereas mechanical injury led to a profound suppression of AMPK phosphorylation at 24 h (Fig. 6*B*). Conversely, p5RHH-p65 siRNA NP administration led to enhanced AMPK phosphorylation in chondrocytes surrounding the area of impact whereas scrambled siRNA had no effect (Fig. 6*B*). Increase in AMPK activity was confirmed by the phosphorylation of its classic target, acetyl-coA carboxylase (Fig. S5*A*). Although compression loading did not significantly change AMPK level, p5RHH-p65 siRNA nanotherapy enhanced total AMPK expression as well as its activity (Fig. S5*B*).

AMPK has also been shown to modulate the Wingless Int-1 (Wnt) signaling pathway (23–25), which is implicated in the pathogenesis of OA (26). Wnt stimulation in cartilage promotes the accumulation and nuclear translocation of β-catenin, an effector of Wnt signaling, where it activates the expression of catabolic target genes such as metalloproteinases (26). We observed an increase in β-catenin level and its nuclear translocation, suggesting that impact injury activated Wnt signaling in chondrocytes (Fig. 6*C*). On the other hand, p5RHH-p65 siRNA nanotherapy significantly suppressed β-catenin expression (Fig. 6*C*).

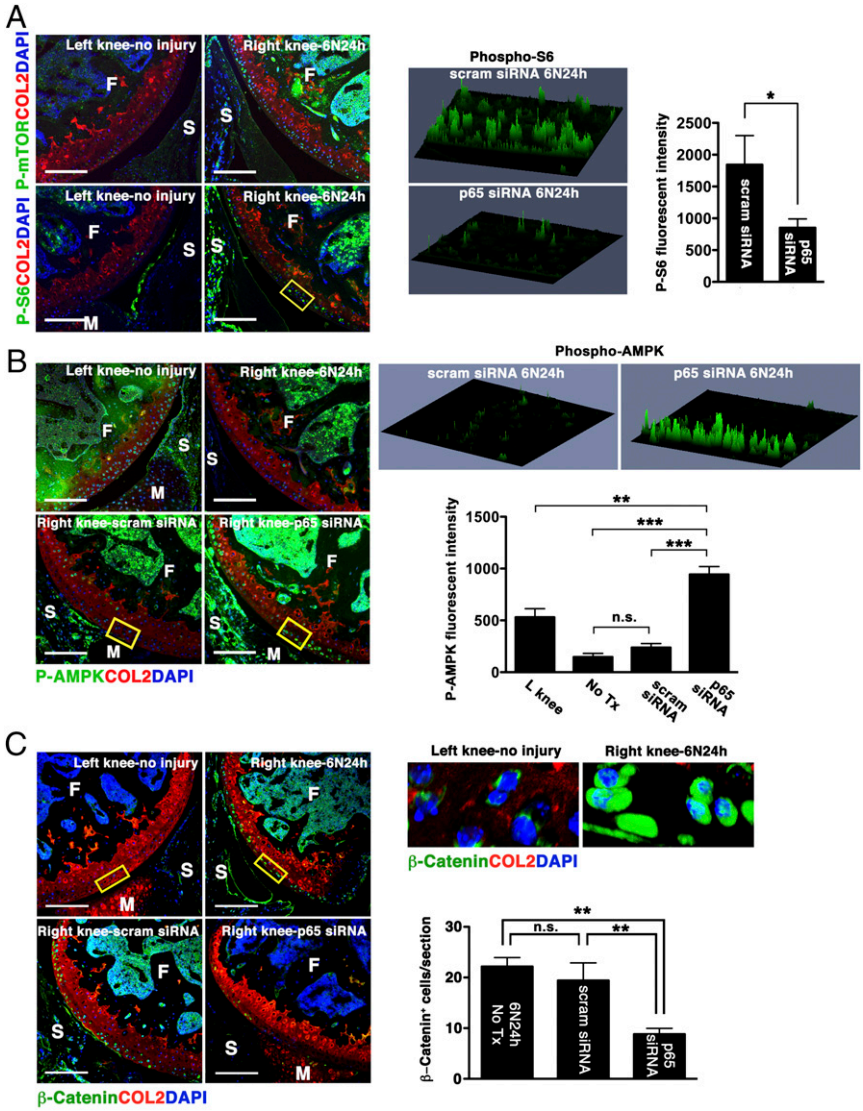

Fig. 6. Effect of p5RHH-p65 siRNA NP on AMPK/mTOR/β-catenin activity. Mice were subjected to compression injury at 6 N and injected i.a. immediately with 0.1 μg of p5RHH-p65 siRNA NPs or p5RHH-scrambled (scram) siRNA NPs, and knees were harvested at 24 h. (*A*) Impact injury up-regulated mTOR activity and phosphorylation of S6. (*B*) AMPK is constitutively activated (left knee); mechanical loading led to profound down-regulation of AMPK activity (right knee). p5RHH-p65 siRNA NP significantly enhanced AMPK phosphorylation. Phospho-S6 and phospho-AMPK intensity in the boxed areas was obtained from z-stack confocal images. (*C*) Impact injury augmented β-catenin level leading to its nuclear translocation whereas p5RHH-p65 siRNA NP administration suppressed its level. The number of chondrocytes with nuclear β-catenin was enumerated across the entire impact area. Values represent mean ± SEM; $n = 3$ mice per treatment (Tx) group. COL2 (red), type II collagen; F, femur; M, meniscus; S, synovium; T, tibia. DAPI (blue) stains nuclei. (Scale bars, 100 μm.) $^{*}P < 0.05$; $^{**}P < 0.01$; $^{***}P < 0.001$; n.s., not significant.

Extended in Vivo Effects of p5RHH–NF-κB siRNA NP. We have shown that p5RHH–NF-κB siRNA nanotherapy attenuated early chondrocyte apoptosis and reactive synovitis at day 5. However, the lasting effect of NF-κB siRNA in the joint following i.a. administration of NP is unknown. To further elucidate this point, we treated a set of mice with three serial doses of p5RHH-p65 siRNA NP delivered i.a. immediately after impact injury and again on days 1 and 2 during the acute phase that was marked by vigorous inflammatory response; p5RHH-scrambled siRNA NP served as control. The knees were harvested on day 14 and analyzed for the number of TUNEL$^+$-positive cells and LC3 expression. Serial p5RHH-p65 siRNA NP treatments significantly preserved chondrocyte viability (~50% reduction in TUNEL$^+$ cells) and homeostasis (~30% reduction in LC3 suppression) (Fig. 7*A*). These results suggest that i.a. administration of p5RHH-p65 siRNA NP partially suppressed the downstream negative effects of impact injury on cartilage (summarized in Fig. 7*B*), an outcome that persisted for at least 2 wk, far beyond the observed short half-life of siRNAs in the circulation (27).

Repeated i.a. injections of p5RHH-p65 siRNA NP did not elicit antibody production (Fig. S6*A*), corroborating our previous data following systemic NP administration (10). In addition, siRNAs have the potential to stimulate pattern recognition receptors such as intracellular toll-like receptors (TLRs), leading to the induction of cytokines that include type I interferons (IFNs) (28). To examine whether i.a. injection of peptide-siRNA NP stimulated type I IFN release, we administered p5RHH-p65 siRNA NP i.a. and examined IFN-stimulated gene (ISG) response in the liver by real-time PCR. Systemic administration of poly(I:C) served as a positive control for TLR stimulation. We found no evidence of type I IFN activation following i.a. injection of p5RHH-p65 siRNA NP (Fig. S6*B*).

Penetration and Persistence of p5RHH-siRNA NP in Human OA Cartilage. As a proof of concept that our results could eventually translate to clinical applications, we tested the efficiency of our p5RHH-siRNA NP penetration in human OA cartilage. Fluorescent-labeled p5RHH-siRNA NPs at 500 nM siRNA concentration (equivalent to the concentration of NPs to which mouse cartilage was exposed in vivo) were incubated with 5-mm^2 cartilage explants from human OA knee joints obtained at the time of total joint arthroplasty. After 48 h of incubation, cartilage explants were washed extensively and processed for histology. Sagittal sections were examined in the central area (to avoid assessment of NP diffusion from the cut sides of the cartilage discs) and evaluated for

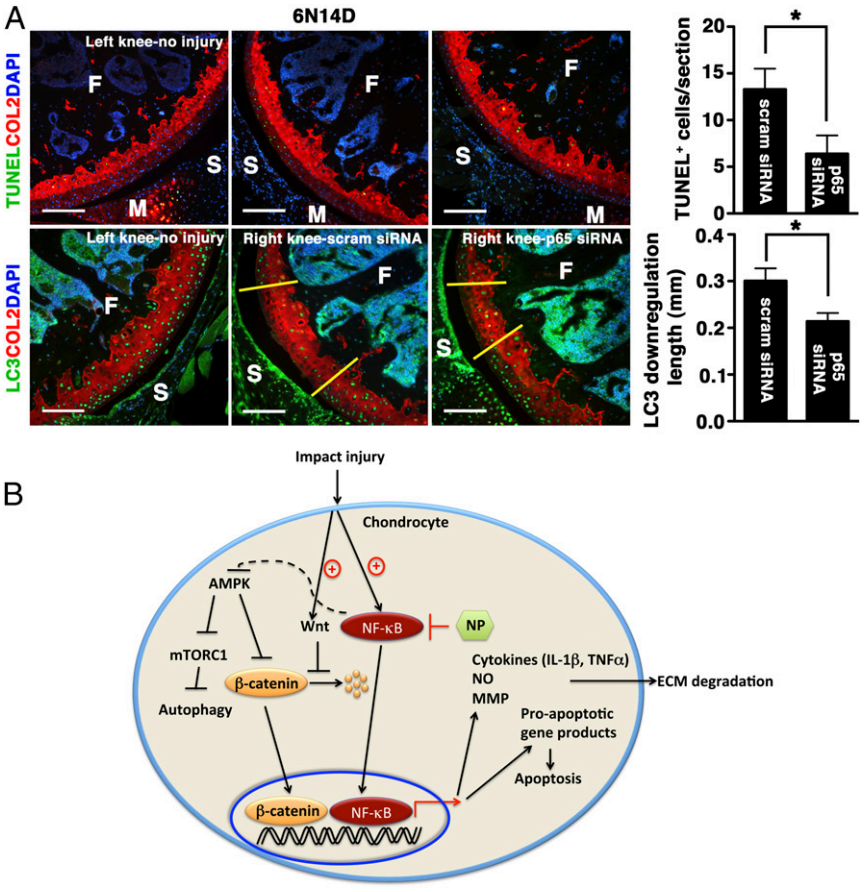

Fig. 7. Extended effects of p5RHH-p65 siRNA NP on cartilage. (*A*) Mice were subjected to compression injury at 6 N and injected immediately i.a. with 0.1 μg of p5RHH-p65 or p5RHH-scrambled (scram) siRNA NP; the dose was repeated at 24 h and at 48 h (for a total of three doses). On day 14, knees were harvested and analyzed for TUNEL$^+$ cells (green, *Upper*) and length of LC3 down-regulation (green: *Lower*, between yellow demarcation lines). Note that the number of TUNEL$^+$ cells decreased over time. Values represent mean ± SEM; $n = 4$ mice per treatment (Tx) group. COL2 (red), type II collagen; F, femur; M, meniscus; S, synovium. DAPI (blue) stains nuclei. (Scale bars, 100 μm.) *$P < 0.05$. (*B*) Graphical summary. Impact injury activates NF-κB–signaling pathways in chondrocytes, leading to expression of inflammatory cytokines that promote ECM degradation and expression of proapoptotic gene products that induce apoptosis. Administration of p5RHH–NF-κB siRNA NP blocks these downstream effects. p5RHH–NF-κB siRNA nanotherapy also potentially preserves chondrocyte/cartilage homeostasis through AMPK activation that, in turn, blocks mTORC1, thus enhancing autophagy. Impact injury likely stimulates Wnt signaling, as evidenced by increased β-catenin level and nuclear translocation. p5RHH–NF-κB siRNA nanotherapy suppresses β-catenin expression, thus reducing the expression of catabolic genes (such as metalloproteinases).

depth of NP penetration by confocal microscopy. In human OA cartilage, NP could be seen in large aggregates within the superficial layer, potentially due to NP accumulation within areas of cartilage fibrillation (Fig. 8*A*). NP could be seen penetrating human OA cartilage up to a depth of at least 700 μm, freely diffusing into chondrocyte lacunae located in the intermediate zone (Fig. 8*B*). NP also deeply penetrated normal cartilage (Fig. S7). To further assess for persistence of siRNAs in cartilage, we incubated OA explants with the same concentration of NP used above, washed off the excess NP after 48 h, and examined for signal from fluorescent-labeled siRNA over time. siRNA fluorescent signal persisted in chondrocyte lacunae for at least 14 d after excess NP removal and could still be detected at low level up to day 21 (Fig. 8*C*).

Discussion

Our results suggest extensive crosstalks between NF-κB and the signaling pathways that govern early cartilage responses to injury (summarized in Fig. 7*B*), thus providing a rationale for suppressing NF-κB activity in limiting the progression of cartilage degeneration.

Growing evidence suggests that the NF-κB pathway is the central regulator of the inflammatory responses in OA (6), yet targeted therapeutic strategies to inhibit NF-κB activity in vivo to slow or reverse OA progression remain far and few between. The i.a. delivery of decoy oligodeoxynucleotides (ODNs) that selectively block NF-κB activation has been previously shown to partially limit the progression of OA induced by surgical transection of the anterior cruciate ligament (29). However, therapeutic delivery of free ODNs is still strongly hampered by a short half-life (30). Another study showed that the use of an adenoviral vector to deliver NF-κB p65 siRNA into knee joints alleviated inflammation and reduced cartilage degradation in a rat surgical model of chronic OA (31). Despite the excellent transfection efficiency attained with viral-based vectors, several safety concerns remain, including genotoxicity and immunogenicity (32). In addition, viral vectors are difficult to produce and have restricted target-cell specificity (33). Nonviral platforms have thus emerged as viable alternatives for siRNA delivery.

The historical challenge of safely delivering therapeutic siRNA in effective doses to selected pathologies is well known (34, 35). The recent resurgence of interest in siRNA delivery by the pharmaceutical industry has focused on agents that accumulate passively in the liver based on the propensity of lipid carriers to be cleared by the reticuloendothelial system (i.e., inhibition of hepatic

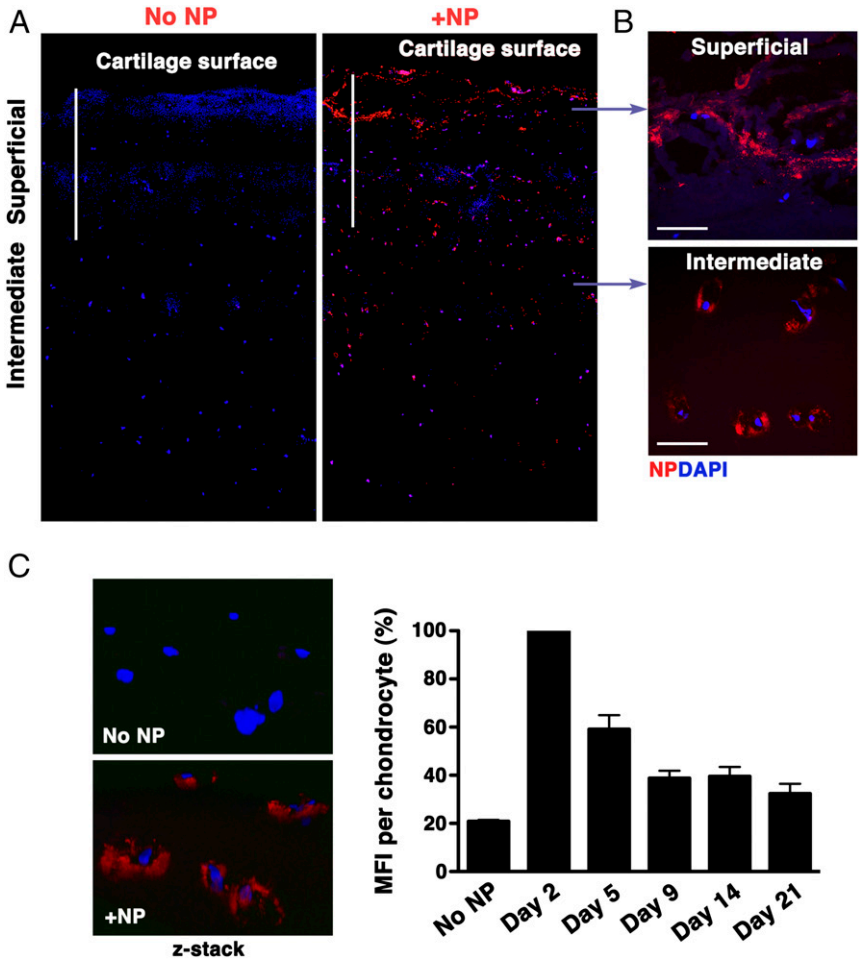

Fig. 8. NP penetration in human OA cartilage explants. p5RHH-Cy3–labeled siRNA NPs (red) were incubated with 5-mm^2 cartilage explants from human OA knee. (*A*) After 48 h, cartilage explants were washed extensively and processed for histology. Sagittal sections were examined for depth of NP penetration by confocal microscopy. DAPI (blue) stains nuclei. (*B*) Large aggregates of NPs could be seen in the matrix of the superficial zone and accumulated in chondrocytes in the intermediate zone. (*C*) Human OA cartilage explants were incubated with fluorescent NPs for 48 h; the excess NP was washed off, and explants were kept in complete culture medium for up to 21 d. Fluorescent signal inside chondrocytes was examined by confocal microscopy at different time points. MFI per chondrocyte was obtained from z-stack confocal images (at least 20 chondrocytes per time point were analyzed); data were derived from two different OA samples. The rate of fluorescence decay was calculated relative to the signal observed on day 2, which was set at 100%. [Scale bars, 500 μm (*A*) and 50 μm (*B*).]

PCSK9 for hypercholesterolemia or transthyretin for familial amyloidosis). To circumvent the shortcomings of lipid carriers, we used a peptidic NP structure that represents the culmination of a number of specific sequence modifications to the amphipathic cationic peptide, melittin (12, 36, 37). In this present version of the peptide, the pore-forming capacity has been intentionally attenuated while still permitting membrane penetration, thus facilitating endosomal escape and coordinated release of siRNA into cytoplasm to avoid deactivation of therapeutic moieties (8, 9, 11, 38). We have previously shown that these particles did not elicit any systemic or adaptive immune responses in an experimental model of rheumatoid arthritis (10). Here, we show that they did not initiate antibody production or stimulate type I IFN response following repeated i.a. injections. p5RHH-siRNA NP freely penetrated avascular human OA cartilage to reach chondrocytes residing in the deeper layers. Moreover, siRNA fluorescent signal persisted for at least 2 wk in chondrocyte lacunae, which may potentially serve as a drug reservoir. Combined with a relatively favorable toxicity profile, these results suggest that p5RHH-siRNA NP merits further consideration for clinical application as a DMOAD platform.

The NF-κB family consists of five members: p105 (constitutively processed to p50), p100 (processed to p52 under-regulated conditions), p65 (also known as RelA), RelB, and c-Rel. These members form homo- and heterodimers that, in the resting cell, are normally held inactive in the cytoplasm by the association with inhibitors, the IκB proteins. Activation of NF-κB is controlled by the IκB kinase complex that phosphorylates IκB proteins and targets them for degradation, releasing the NF-κB subunits for nuclear translocation and transactivation of a multitude of responsive genes. We confirmed that the p65 canonical pathway of NF-κB plays a major role in regulating the early molecular events following mechanical loading. Although p100 may also participate in these inflammatory responses, we found that dual inhibition of p65 and p100 activities did not provide a net overall advantage to the individual approach of p65 knockdown. This may be explained by the fact that p52 (the processed form of p100) can heterodimerize to either p50 or p65 and act as a transcription repressor or activator, respectively (39). Thus, p100 silencing may exhibit mixed anti- and proinflammatory effects. In the future, we plan to explore selective inhibition of NF-κB–inducible kinase as this is the most important regulatory kinase of the noncanonical pathway (40).

NF-κB is known to modulate cell survival and apoptosis. NF-κB has long been regarded as a transcription factor that prevents TNFα-induced cell death by inducing the expression of antiapoptotic genes (41–44). However, NF-κB may also play a proapoptotic function, depending on the stimulus and cellular environment. A number of studies have suggested the involvement of NF-κB in apoptosis of articular chondrocytes through a nitric oxide (NO)-dependent mechanism (45, 46). NO in articular chondrocytes induces activation of p38 leading to NF-κB signaling, which in turn increases expression of proapoptotic members of the Bcl-2 family. We hypothesized that biomechanical injury leads to NF-κB activation, triggering a cascade of events in chondrocytes that includes the release of inflammatory mediators, which perpetuate the catabolic cycles leading to chondrocyte apoptosis. Congruent with this hypothesis, we found that suppression of NF-κB activity significantly protects against chondrocyte apoptosis in addition to suppressing the inflammation that drives reactive synovitis.

mTOR is a signaling pathway that promotes cell growth and differentiation while inhibiting cellular catabolism by blocking autophagy (18). Genetic ablation of cartilage mTOR (47) or inhibition of mTOR with the drug rapamycin (48, 49) reduces the expression of catabolic enzymes and maintains cartilage viability in experimental OA. Here we establish that mTORC1 is activated early (within 24 h) in chondrocytes following a mechanical injury. A variety of upstream signals converge on mTORC1, and one of these signals is AMPK (18). AMPK acts as a "central regulator" of inflammatory signaling in various cell types (50–52). In addition, AMPK activation has been shown to reduce inflammation in vivo in several preclinical models (53–55). The activation of AMPK is known to inhibit mTOR-dependent signaling activity (18). Although ample evidence indicates that AMPK activation inhibits NF-κB signaling via several pathways (56), whether NF-κB can conversely modulate AMPK activity in chondrocytes has not been examined. Our data suggest that compression injury activates NF-κB while suppressing AMPK activity, which may allow uninhibited mTORC1 activity to repress autophagy. In contrast, p5RHH–NF-κB siRNA nanotherapy enhances AMPK activity and suppresses mTORC1, thus preserving chondrocyte autophagic activity and homeostasis. Although the exact mechanism by which NF-κB modulates AMPK activity remains to be determined, we envision that NF-κB–induced proinflammatory cytokines such as IL-1β and TNFα may negatively regulate the activity of AMPK (22). However, we cannot exclude the possibility that p5RHH-NF-κB siRNA NP administration affects other signaling pathways that activate AMPK. We also cannot exclude that other factors, such as Wnt signaling, may affect mTORC1 activity (18).

The canonical Wnt/β-catenin–signaling pathway plays a critical role in the development and maintenance of bone and cartilage (26). Polymorphisms in certain Wnt genes increase susceptibility to OA whereas higher expression of Wnt pathway antagonists may delay OA progression (26). β-Catenin, the effector of canonical Wnt signaling, is normally sequestered in a protein complex that negatively regulates its activity, accelerating its degradation (26). Wnt stimulation releases β-catenin from this regulatory complex, blocking its degradation and allowing it to translocate to the nucleus. Conversely, AMPK has been shown to suppress Wnt signaling by up-regulating β-catenin degradation (24). Our studies showed that p5RHH–NF-κB siRNA nanotherapy augmented AMPK activity while suppressing β-catenin level and nuclear translocation. These results support a crosstalk between NF-κB and Wnt, perhaps through AMPK-mediated modulation of the β-catenin level, although determining the exact mechanism will require further studies.

In summary, our study shows that p5RHH–NF-κB siRNA nanotherapy mediates chondroprotective effect partially by maintaining cartilage autophagy/homeostasis via modulation of AMPK, mTORC1, and Wnt/β-catenin activity. Because NF-κB–mediated chondrocyte differentiation and disruption of cartilage homeostasis are also characteristics of primary OA (6, 57), our findings suggest that modulation of this pathway may potentially impact the progression of cartilage degeneration in general. However, the optimal timing and schedule for targeted anti–NF-κB therapy in primary OA will require further studies.

Materials and Methods

p5RHH-siRNA NP Preparation. p5RHH peptide (provided by Genscript) was dissolved at 10 mM in DNase-, RNase-, and protease- free sterile purified water (Cellgro) and stored in 10-μL aliquots at −80 °C before use. The Cy5.5-labeled scrambled siRNAs and Cy3-labeled p65 siRNAs were procured from Sigma-Aldrich, dissolved at 100 μM in 1× siRNA buffer (Thermo Scientific), and stored in 10-μL aliquots at −80 °C before use. The p5RHH siRNA NPs were prepared by mixing equal volumes of the aforementioned p5RHH peptide and siRNA at a peptide/siRNA ratio of 100:1 in HBSS with Ca^{2+} and Mg2+ (Gibco and Life Technologies) and incubated at 37 °C for 40 min and then stabilized with albumin at a final siRNA concentration of 500 nM before i.a. injection or incubated on ice for 10 min before adding to the cartilage culture. This preparation typically results in a nominal NP size of ∼55 nm after applying a stabilizing albumin coating, as measured by atomic force microscopy, and zeta potentials varying from +12 to −5.5 mV and a polydispersity index varying from 0.120 to 0.190 depending on size and the presence or absence of an exogenously applied albumin coating. We also have previously shown that the uncoated particles are slightly smaller (by 14%) than the albumin-coated particles by dynamic light scattering (8, 9).

TEM on p5RHH-siRNA NPs. For visualizing the p5RHH-siRNA NPs, the electron microscopy mesh copper grids (S160-4) were negatively charged by glow

discharge. p5RHH-siRNA NPs were diluted 10 times and then incubated with the grid for 1 min. After the incubation, the grids were washed with distilled water and then gently blotted dry, followed by staining with 2% phosphotungstic acid for 30 s. The p5RHH-siRNA NP samples were viewed on a JEOL 1200 EX II transmission electron microscope.

Noninvasive Mechanical Injury Model. Mice were kept in a pathogen-free condition at the Washington University Specialized Research Facility and were used in experiments that were approved by the Animal Studies Committee.

Experiments were performed on 8-wk-old male C57BL/6J mice (The Jackson Laboratory) using a materials testing machine (Instron ElectroPuls E1000) as previously described (5). Briefly, under anesthesia, the right tibiae were positioned with the knee downward in deep flexion between custom-made cups and subjected to axial compressive loads with a peak force of 6 Newtons (N) with a 0.5 N preload force to maintain the limb in position between loading cycles. Cyclic loads were applied for 0.34 s with a rise and fall time each of 0.17 s and a baseline hold time of 10 s between cycles for 60 cycles. The uninjured left knees were used as controls. Some animals received an i.a. dose of NPs immediately after loading that may be repeated at 24 h and/or 48 h. Animals were returned to their cages after loading and were given standard mouse chow and water ad libitum. At indicated time points after injury, knee joints were dissected, fixed in formalin, paraffin-embedded, and processed for histological analysis.

NP Administration. NPs were administered using sterile techniques: the knee was kept in a flexed position and a volume of 15 μL of p5RHH-siRNA NP (0.1 μg, which is equivalent to siRNA at 7.5×10^{-12} mol) was injected i.a. using a 30-gauge needle. The left knees served as controls. The injections were repeated at 24 h and/or 48 h. Some of the knee joints were harvested at 12, 24, and 48 h or at days 5, 9, and 14 after the loading.

Histological Analysis of Mouse Knee Joints. Formalin-fixed knee joints were decalcified and embedded in paraffin for sectioning. Serial sagittal sections (5 μm in thickness) from individual knees were cut through the entire lateral femoral condyle as described previously (5). Selected sections were stained with Safranin O-fast green (to evaluate articular cartilage proteoglycan content), according to standard protocols. The length of the cartilage injury (loss of Safranin O staining) in each individual knee was measured using ImageJ software (https://imagej.nih.gov/ij) based on the section with the most severe injury. Postinjury reactive synovitis was scored on a scale of 0–3 using an established scoring system described previously (5): 0—normal thickness of synovial lining (1–2 cells); 1, 2—thickness of 2–4 cells; 2—thickness of 4–9 cells; and 3—thickness ≥10 cells. Quantitative scoring was performed in a blinded fashion.

Detection of Chondrocyte Apoptosis. Detection of apoptotic cells was performed using an In Situ Cell Death Detection Kit with Fluorescein (catalog no. 11–684-795–910, Roche) with the TUNEL assay. Briefly, paraffin-embedded knee sections were deparaffinized, rehydrated, treated with protease K (10 μg/mL for 20 min at 37 °C), and permeabilized with 0.5% TWEEN-20/PBS for 15 min. A freshly prepared TUNEL reaction mixture was applied to sections for 60 min at 37 °C, rinsed three to five times with PBS, and mounted with VECTASHIELD mounting medium with DAPI (catalog no. H-1200, Vector Laboratories). The $TUNEL^+$ cell number cells were enumerated across the entire impact area and expressed as a mean.

Immunofluorescence Staining and Confocal Microscopy. Paraffin sections were deparaffinized and rehydrated. Sections were incubated with 3% (vol/vol) H_2O_2 in PBS for 15 min to quench endogenous peroxidases. Proteinase K (10 μg/mL for 20 min at 37 °C) was applied to the sections for antigen retrieval. After blocking endogenous biotin (Avidin/Biotin Blocking Kit, Vector Laboratories) and Tyramide Signal Amp (TSA) blocking solution for 1 h at room temperature, slides were incubated with the primary antibodies anti-LC3 (1:100, catalog no. L7543, Sigma-Aldrich), phospho-p65 (1:100, ab28856, Abcam), phospho-p100 (1:100, catalog no. orb106199, Biorbyt), phospho-mTOR (1:100, catalog no. 5536, Cell Signaling), phospho-S6 Ribosomal Protein (1:100, catalog no. 4858, Cell Signaling), AMPK (1:100, catalog no. ab131512, Abcam), phospho-AMPK (1:100, catalog no. 1535, T172, Cell Signaling), β-catenin (1:100, catalog no. ab16051, Abcam), (1:100, catalog no. 11818, Cell Signaling), cleaved PARP (1:100, catalog no. 9544, Cell Signaling), and aggrecan (1:200, catalog no. AB1031, Millipore) diluted in TSA block buffer overnight at 4 °C and then washed and incubated with the corresponding HRP-conjugated secondary antibodies. Biotinyl Tyramide working solution (1:100) was applied for 3–10 min to enhance the specific signal of primary antibodies. All of the sections were incubated in Alexa Fluor 488-conjugated–streptavidin (1:200, catalog no. S-11223, Molecular Probes) diluted in TSA blocking buffer for 30 min at room temperature and counterstained with DAPI (1:1,000, Vector Laboratories). Slides were subsequently incubated with COL2 antibody (1:200, generously provided by L. J. Sandell and M. F. Rai, Washington University, St. Louis) (5) for 1 h at room temperature followed by TRITC-conjugated anti-rat secondary antibody (1:100, catalog no. 712–295-153, Jackson ImmunoResearch). All images were visualized on a Nikon ECLIPSE microscope and acquired with QCapture software or ZEISS LSM 880 Confocal Laser Scanning Microscope. The quantification of phospho-p65, phospho-p100, phospho-S6, phospho- and total AMPK, and phospho-ACC was performed with software ZEN, and the analyzed chondrocytes were chosen at a site immediately outside of the impact area. The data were obtained from 15 to 20 cells per section and 3–4 sections per knee joint and presented as the average mean fluorescent intensity per cell. Quantitative scoring was performed in a blinded fashion.

Ex Vivo Culture of Cartilage Explants. Human cartilage explants were obtained from patients who signed consent forms at the time of total knee arthroplasty through a protocol approved by the Institutional Review Board at Washington University School of Medicine and provided to us for these studies anonymously. The explants were then washed several times with HBSS containing antibiotics, incubated overnight in culture medium containing DMEM/F12 (1:1), 10% FBS, penicillin/streptomycin (100 U/0.1 mg/mL), amphotericin B (0.25 μg/mL), and ciprofloxin (10 μg/mL) in a six-well plate at 37 °C and 5% CO_2. One day after incubation, cartilage explants were placed in a 96-well plate and incubated with p5RHH-Cy3–labeled siRNA NPs in 250 μL of culture medium (which rendered the siRNA at a concentration of 500 nM) and incubated for 48 h. After three to five washes with PBS, the cartilage explants either were embedded in Tissue-Tek Optimal Cutting Temperature (O.C.T.) compound (Sakura Finetek USA, Inc.) or further cultured in complete culture medium without NPs. At specific time points (5, 9, 14, and 21 d) the explants were again washed extensively and embedded in O.C.T. compound. The nonfixed sections were directly mounted with VECTASHIELD mounting medium with DAPI (catalog no. H-1200, Vector Laboratories), and images were acquired using confocal microscopy.

Statistics. Comparisons between multiple groups (three or more) were performed by one-way ANOVA, and Bonferroni's correction for multiple comparisons was performed. The sample size (number of animals per genotype/treatment) chosen is based on means and variances in similar experiments in this mouse model of OA for detection of differences between experimental groups at an α-level of 0.05 and a statistical power of 0.80, assuming a two-sided test.

ACKNOWLEDGMENTS. We thank Dr. R. Nunley (Washington University) for providing discarded human OA tissues; Dr. M. Silva (Washington University) for the use of the materials-testing machine for the loading procedure; and Crystal Idleburg for excellent histological tissue processing. This work was partially supported by NIH Grants R01AR067491 (to C.T.N.P.), R01HL073646 and R01DK102691 (to S.A.W.), P30AR057235 (to L.E.S.), K99 AR064837 (to M.F.R.), and F32 AR064667 (to N.H.). The content is solely the responsibility of the authors and does not necessarily represent the official views of the NIH.

1. Hootman JM, Helmick CG (2006) Projections of US prevalence of arthritis and associated activity limitations. *Arthritis Rheum* 54(1):226–229.
2. Brown TD, Johnston RC, Saltzman CL, Marsh JL, Buckwalter JA (2006) Posttraumatic osteoarthritis: A first estimate of incidence, prevalence, and burden of disease. *J Orthop Trauma* 20(10):739–744.
3. Chalmers PN, et al. (2014) Does ACL reconstruction alter natural history?: A systematic literature review of long-term outcomes. *J Bone Joint Surg Am* 96(4):292–300.
4. Lieberthal J, Sambamurthy N, Scanzello CR (2015) Inflammation in joint injury and post-traumatic osteoarthritis. *Osteoarthritis Cartilage* 23(11):1825–1834.
5. Wu P, et al. (2014) Early response of mouse joint tissue to noninvasive knee injury suggests treatment targets. *Arthritis Rheumatol* 66(5):1256–1265.
6. Marcu KB, Otero M, Olivotto E, Borzi RM, Goldring MB (2010) NF-kappaB signaling: Multiple angles to target OA. *Curr Drug Targets* 11(5):599–613.
7. Setton L (2008) Polymer therapeutics: Reservoir drugs. *Nat Mater* 7(3):172–174.
8. Hou KK, Pan H, Lanza GM, Wickline SA (2013) Melittin derived peptides for nanoparticle based siRNA transfection. *Biomaterials* 34(12):3110–3119.
9. Hou KK, Pan H, Ratner L, Schlesinger PH, Wickline SA (2013) Mechanisms of nanoparticle-mediated siRNA transfection by melittin-derived peptides. *ACS Nano* 7(10):8605–8615.
10. Zhou HF, et al. (2014) Peptide-siRNA nanocomplexes targeting NF-κB subunit p65 suppress nascent experimental arthritis. *J Clin Invest* 124(10):4363–4374.
11. Pan H, et al. (2010) Lipid membrane editing with peptide cargo linkers in cells and synthetic nanostructures. *FASEB J* 24(8):2928–2937.

12. Pan H, et al. (2011) Post-formulation peptide drug loading of nanostructures for metered control of NF-κB signaling. *Biomaterials* 32(1):231–238.
13. Pan H, et al. (2013) Programmable nanoparticle functionalization for in vivo targeting. *FASEB J* 27(1):255–264.
14. Caramés B, Taniguchi N, Otsuki S, Blanco FJ, Lotz M (2010) Autophagy is a protective mechanism in normal cartilage, and its aging-related loss is linked with cell death and osteoarthritis. *Arthritis Rheum* 62(3):791–801.
15. Sasaki H, et al. (2012) Autophagy modulates osteoarthritis-related gene expression in human chondrocytes. *Arthritis Rheum* 64(6):1920–1928.
16. Trocoli A, Djavaheri-Mergny M (2011) The complex interplay between autophagy and NF-κB signaling pathways in cancer cells. *Am J Cancer Res* 1(5):629–649.
17. Baldwin AS (2012) Regulation of cell death and autophagy by IKK and NF-κB: Critical mechanisms in immune function and cancer. *Immunol Rev* 246(1):327–345.
18. Laplante M, Sabatini DM (2012) mTOR signaling in growth control and disease. *Cell* 149(2):274–293.
19. Meley D, et al. (2006) AMP-activated protein kinase and the regulation of autophagic proteolysis. *J Biol Chem* 281(46):34870–34879.
20. Inoki K, Kim J, Guan KL (2012) AMPK and mTOR in cellular energy homeostasis and drug targets. *Annu Rev Pharmacol Toxicol* 52:381–400.
21. Bohensky J, Leshinsky S, Srinivas V, Shapiro IM (2010) Chondrocyte autophagy is stimulated by HIF-1 dependent AMPK activation and mTOR suppression. *Pediatr Nephrol* 25(4):633–642.
22. Terkeltaub R, Yang B, Lotz M, Liu-Bryan R (2011) Chondrocyte AMP-activated protein kinase activity suppresses matrix degradation responses to proinflammatory cytokines interleukin-1β and tumor necrosis factor α. *Arthritis Rheum* 63(7):1928–1937.
23. Zhao J, Yue W, Zhu MJ, Sreejayan N, Du M (2010) AMP-activated protein kinase (AMPK) cross-talks with canonical Wnt signaling via phosphorylation of beta-catenin at Ser 552. *Biochem Biophys Res Commun* 395(1):146–151.
24. Takatani T, Minagawa M, Takatani R, Kinoshita K, Kohno Y (2011) AMP-activated protein kinase attenuates Wnt/β-catenin signaling in human osteoblastic Saos-2 cells. *Mol Cell Endocrinol* 339(1-2):114–119.
25. Zhao JX, Yue WF, Zhu MJ, Du M (2011) AMP-activated protein kinase regulates beta-catenin transcription via histone deacetylase 5. *J Biol Chem* 286(18):16426–16434.
26. Corr M (2008) Wnt-beta-catenin signaling in the pathogenesis of osteoarthritis. *Nat Clin Pract Rheumatol* 4(10):550–556.
27. Naeye B, et al. (2013) In vivo disassembly of IV administered siRNA matrix nanoparticles at the renal filtration barrier. *Biomaterials* 34(9):2350–2358.
28. Kanasty RL, Whitehead KA, Vegas AJ, Anderson DG (2012) Action and reaction: The biological response to siRNA and its delivery vehicles. *Mol Ther* 20(3):513–524.
29. Roman-Blas JA, Jimenez SA (2006) NF-kappaB as a potential therapeutic target in osteoarthritis and rheumatoid arthritis. *Osteoarthritis Cartilage* 14(9):839–848.
30. De Stefano D (2011) Oligonucleotides decoy to NF-kappaB: Becoming a reality? *Discov Med* 12(63):97–105.
31. Chen LX, et al. (2008) Suppression of early experimental osteoarthritis by in vivo delivery of the adenoviral vector-mediated NF-kappaBp65-specific siRNA. *Osteoarthritis Cartilage* 16(2):174–184.
32. Wang D, Gao G (2014) State-of-the-art human gene therapy: Part I. Gene delivery technologies. *Discov Med* 18(97):67–77.
33. Chira S, et al. (2015) Progresses towards safe and efficient gene therapy vectors. *Oncotarget* 6(31):30675–30703.
34. Castanotto D, Rossi JJ (2009) The promises and pitfalls of RNA-interference-based therapeutics. *Nature* 457(7228):426–433.
35. Merkel OM, et al. (2011) Polymer-related off-target effects in non-viral siRNA delivery. *Biomaterials* 32(9):2388–2398.
36. Soman NR, et al. (2009) Molecularly targeted nanocarriers deliver the cytolytic peptide melittin specifically to tumor cells in mice, reducing tumor growth. *J Clin Invest* 119(9):2830–2842.
37. Soman NR, Lanza GM, Heuser JM, Schlesinger PH, Wickline SA (2008) Synthesis and characterization of stable fluorocarbon nanostructures as drug delivery vehicles for cytolytic peptides. *Nano Lett* 8(4):1131–1136.
38. Hou KK, Pan H, Schlesinger PH, Wickline SA (2015) A role for peptides in overcoming endosomal entrapment in siRNA delivery: A focus on melittin. *Biotechnol Adv* 33(6 Pt 1):931–940.
39. Hoesel B, Schmid JA (2013) The complexity of NF-κB signaling in inflammation and cancer. *Mol Cancer* 12:86.
40. Noort AR, Tak PP, Tas SW (2015) Non-canonical NF-κB signaling in rheumatoid arthritis: Dr Jekyll and Mr Hyde? *Arthritis Res Ther* 17:15.
41. Beg AA, Baltimore D (1996) An essential role for NF-kappaB in preventing TNF-alpha-induced cell death. *Science* 274(5288):782–784.
42. Wang CY, Mayo MW, Baldwin AS, Jr (1996) TNF- and cancer therapy-induced apoptosis: Potentiation by inhibition of NF-kappaB. *Science* 274(5288):784–787.
43. Van Antwerp DJ, Martin SJ, Kafri T, Green DR, Verma IM (1996) Suppression of TNF-alpha-induced apoptosis by NF-kappaB. *Science* 274(5288):787–789.
44. Liu ZG, Hsu H, Goeddel DV, Karin M (1996) Dissection of TNF receptor 1 effector functions: JNK activation is not linked to apoptosis while NF-kappaB activation prevents cell death. *Cell* 87(3):565–576.
45. Kim SJ, Hwang SG, Shin DY, Kang SS, Chun JS (2002) p38 kinase regulates nitric oxide-induced apoptosis of articular chondrocytes by accumulating p53 via NFkappa B-dependent transcription and stabilization by serine 15 phosphorylation. *J Biol Chem* 277(36):33501–33508.
46. Kim SJ, Chun JS (2003) Protein kinase C alpha and zeta regulate nitric oxide-induced NF-kappa B activation that mediates cyclooxygenase-2 expression and apoptosis but not dedifferentiation in articular chondrocytes. *Biochem Biophys Res Commun* 303(1): 206–211.
47. Zhang Y, et al. (2015) Cartilage-specific deletion of mTOR upregulates autophagy and protects mice from osteoarthritis. *Ann Rheum Dis* 74(7):1432–1440.
48. Caramés B, et al. (2012) Autophagy activation by rapamycin reduces severity of experimental osteoarthritis. *Ann Rheum Dis* 71(4):575–581.
49. Takayama K, et al. (2014) Local intra-articular injection of rapamycin delays articular cartilage degeneration in a murine model of osteoarthritis. *Arthritis Res Ther* 16(6): 482.
50. Sag D, Carling D, Stout RD, Suttles J (2008) Adenosine 5′-monophosphate-activated protein kinase promotes macrophage polarization to an anti-inflammatory functional phenotype. *J Immunol* 181(12):8633–8641.
51. Yang Z, Kahn BB, Shi H, Xue BZ (2010) Macrophage alpha1 AMP-activated protein kinase (alpha1AMPK) antagonizes fatty acid-induced inflammation through SIRT1. *J Biol Chem* 285(25):19051–19059.
52. Galic S, et al. (2011) Hematopoietic AMPK β1 reduces mouse adipose tissue macrophage inflammation and insulin resistance in obesity. *J Clin Invest* 121(12):4903–4915.
53. Nath N, et al. (2005) 5-Aminoimidazole-4-carboxamide ribonucleoside: A novel immunomodulator with therapeutic efficacy in experimental autoimmune encephalomyelitis. *J Immunol* 175(1):566–574.
54. Zhao X, et al. (2008) Activation of AMPK attenuates neutrophil proinflammatory activity and decreases the severity of acute lung injury. *Am J Physiol Lung Cell Mol Physiol* 295(3):L497–L504.
55. Bai A, et al. (2010) AMPK agonist downregulates innate and adaptive immune responses in TNBS-induced murine acute and relapsing colitis. *Biochem Pharmacol* 80(11):1708–1717.
56. Salminen A, Hyttinen JM, Kaarniranta K (2011) AMP-activated protein kinase inhibits NF-κB signaling and inflammation: Impact on healthspan and lifespan. *J Mol Med (Berl)* 89(7):667–676.
57. Shapiro IM, Layfield R, Lotz M, Settembre C, Whitehouse C (2014) Boning up on autophagy: The role of autophagy in skeletal biology. *Autophagy* 10(1):7–19.